

# Atlas-Based Delineation of Lymph Node Levels in Head and Neck Computed Tomography Images

Olivier Commowick<sup>a,b</sup> Vincent Grégoire<sup>c</sup> Grégoire Malandain<sup>a</sup>

<sup>a</sup>*INRIA Sophia Antipolis - ASCLEPIOS Team, 2004 route des lucioles, BP93,  
06902 Sophia Antipolis Cedex, FRANCE*

<sup>b</sup>*DOSIsoft S.A., 45 avenue Carnot, 94230 Cachan, FRANCE*

<sup>c</sup>*Radiation Oncology Dept., St-Luc University Hospital, Université Catholique de  
Louvain, Brussels, BELGIUM*

---

*Corresponding author:* Olivier Commowick.  
Mail address: INRIA Sophia Antipolis - ASCLEPIOS Team,  
2004 route des lucioles, BP93,  
06902 Sophia Antipolis Cedex, FRANCE.  
E-mail address: ocommowi@gmail.com  
Web site: <http://olivier.commowick.org/>

---

*Keywords:* Anatomical Atlas Construction ; Radiotherapy ; Head and Neck ; Lymph Nodes ; Non linear Registration.

**Abstract**

**Purpose:** Radiotherapy planning requires accurate delineations of the tumor and of the critical structures. Atlas-based segmentation has been shown to be very efficient to automatically delineate brain critical structures. We therefore propose to construct an anatomical atlas of the head and neck region.

**Methods and Materials:** Due to the high anatomical variability of this region, an atlas built from a single image as for the brain is not adequate. We address this issue by building a symmetric atlas from a database of manually segmented images. First, we develop an atlas construction method and apply it to a database of 45 Computed Tomography (CT) images from patients with node-negative pharyngo-laryngeal squamous cell carcinoma manually delineated for radiotherapy. Then, we qualitatively and quantitatively evaluate the results generated by the built atlas based on Leave-One-Out framework on the database.

**Results:** We present qualitative and quantitative results using this atlas construction method. The evaluation was performed on a subset of 12 patients among the original CT database of 45 patients. Qualitative results depict visually well delineated structures. The quantitative results are also good, with an error with respect to the best achievable results ranging from 0.196 to 0.404 with a mean of 0.253.

**Conclusions:** These results show the feasibility of using such an atlas for radiotherapy planning. Many perspectives are raised from this work ranging from extensive validation to the construction of several atlases representing sub-populations, to account for large inter-patient variabilities, and populations with node-positive tumors.

---

**1 Introduction**

The treatment of tumors may involve chemotherapy, surgery or radiotherapy. Owing to recent technological advances, conformal radiotherapy precisely targets the tumor while keeping an acceptable level of irradiation even on nearby critical structures. However, it is necessary to locate accurately the tumor and the organs at risk in order to determine the best characteristics for the irradiation beams. However, a manual delineation process is typically tedious, very long and not always reproducible.

The use of an anatomical atlas, i.e. an image of a mean anatomy and its segmentation, has been extensively studied to automatically delineate the brain for many different applications [1–4]. These methods differ most often by the registration method used to map the atlas image onto the patient. Recently, [5–7] proposed the use of an atlas for the segmentation of brain critical structures for radiotherapy. In this context, many methods have also been introduced to

take into account the presence of the tumor in the brain [8–10] to reduce the tumor induced registration discrepancies.

Tumors in the head and neck region are more frequent than in the brain and represent around 7% of all the cancers. The treatment of these tumors often involves radiotherapy. It would then be of great interest to develop an anatomical atlas to help the physician to segment automatically structures of interest in this region. Recently, consensus guidelines have been presented for the delineation of neck lymph node levels for radiotherapy planning [11,12]. These are based on precise and clearly identifiable anatomical landmarks to determine the limits between the lymph node levels in the patient image. Using an atlas whose anatomy is delineated following these guidelines is therefore of great interest as it would provide the physician with an automatic and reproducible delineation.

Some desirable properties for the atlas have been outlined by Bondiau *et al.* [7] in the case of a brain atlas. They evaluated three atlases for the automatic delineation of the brain.

- An initial atlas was built from an image of a single healthy subject, which was delineated manually by an expert. However, the anatomical variability between patients introduced a systematic error on all segmentations performed.
- To overcome this problem, a second atlas, based on a simulated MRI of an average brain anatomy (coming from the BrainWEB<sup>1</sup> [13–16]), was constructed. Due to the asymmetry of the atlas, however, certain errors remained.
- Finally, a symmetric atlas, derived from an image of a symmetric anatomy (based on the preceding atlas), effectively resolved these errors. Experiments showed this last atlas was the most adapted to the different anatomies.

The observations noted above apply equally, and in some cases more so, to the head and neck region, where various neck positions and degrees of fat may create large differences. Using an atlas built from one manually segmented image may therefore lead to discrepancies when registering one patient on the atlas. We have then chosen to build a symmetric mean atlas from a database of patients manually delineated following the rules given in [11].

This paper is organized as follows: we first describe our image database and methods for atlas construction ; we then present the method we used to build an atlas from a database of images which have been manually delineated. We will then show how this atlas can be used to automatically delineate a patient. In a second part, a Leave-One-Out framework will be associated to our construction method to evaluate quantitatively our atlas-based segmentation

---

<sup>1</sup> <http://www.bic.mni.mcgill.ca/brainweb/>

method. Finally, we will present results of the head and neck atlas construction and evaluation on our CT image database.

## 2 Methods and Materials

### 2.1 Head and Neck Image Database

In this paper, we have used a database of patients with node-negative pharyngolaryngeal squamous cell carcinoma. For that purpose, manually segmented images were provided by the Radiation Oncology Department of the Catholic University of Louvain (UCL). This database consists of 45 CT images with a voxel size of  $1.5 \times 1.5 \times 2 \text{ mm}^3$  acquired in routine clinical practice. For each of these images, structures of interest have been delineated following the guidelines given in [11] for purposes of radiotherapy planning. The available structures for our atlas were the lymph nodes (levels II, III and IV), the parotids, the brainstem, the spinal cord, the mandible and the sub-mandibular glands.

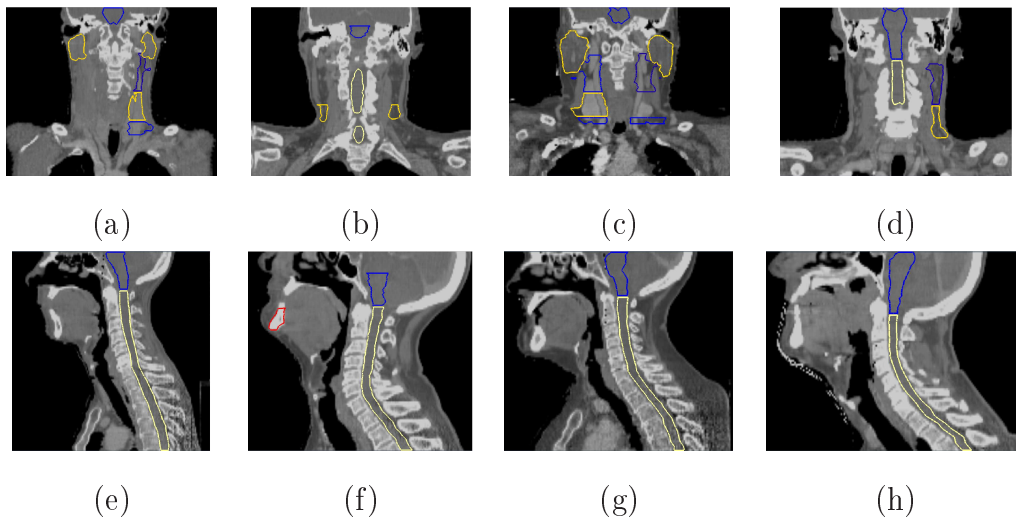


Fig. 1. **Illustration of the image database from UCL.** Examples of sagittal (upper line) and coronal slices (bottom line) and their manual segmentations for 4 patients showing an important variability of position and anatomy.

Some examples illustrating the variability of positions and anatomy between the patients are shown in Fig. 1. Some contours are missing in these patients. Some lymph node levels have indeed been removed because they also included the adjacent primary tumor volume.

## 2.2 Atlas Construction

### 2.2.1 State of the Art

The construction of an atlas from a database of images relies basically on the registration of all the images on a reference image. However, choosing a specific image as the reference introduces a bias due to its specific anatomy. Several methods were therefore introduced to select the atlas as the least biased reference image. Marsland *et al.* [17] selected the reference image as the one that minimizes the sum of the distances with respect to the other images. Park *et al.* [18] proceeded in a similar manner, but used all pairwise registrations between the images to compute the distances.

Other methods were also introduced to build an unbiased atlas [19–21]. They iterate on two steps: the registration of the images on the reference and the application of the inverse mean transformation to the mean image. Guimond *et al.* [19] have shown that this approach, extended by [20,21] to transformations containing large deformations, is not dependent on the choice of the reference image. Recently, based on this principle, a method has been investigated to generate directly a mean symmetric atlas from a database of images [22].

Other methods use higher dimension registration to register simultaneously the images in a common space [23,24]. They optimize a criterion maximizing a similarity measure between the images while minimizing the displacements with respect to the mean image.

Finally, de Craene *et al.* [25] proposed recently a method to build the mean image and compute the mean segmentations together. This is achieved using an EM algorithm which alternates two steps. First, the mean image is estimated by registering the manual segmentations. Then, the mean segmentations are computed using a method similar to STAPLE [26].

### 2.2.2 Construction Method Overview

To create our mean symmetric atlas of the head and neck region, we will use the database of CT images described in section 2.1. In this context, we have chosen not to use the method proposed in [25] because it relies on the registration of manual segmentations without taking into account the CT images. However, in our context, the structures of interest do not cover all of the CT images; hence, the computed transformations outside of these regions will be indeterminate, leading to errors when building the mean CT image. Moreover, the high intra- and inter-patient variability may also introduce errors in the atlas.

For these reasons, we have opted for a more classical, separated approach in

constructing our atlas, as illustrated in Fig. 2. We present in the remainder of this section the main steps of the atlas construction, which can be summed up as follows:

- construction of an asymmetric mean image (section 2.2.3),
- computation of the mean segmentations from the individual manual segmentations (section 2.2.4),
- symmetrization of the atlas generated (section 2.2.5).

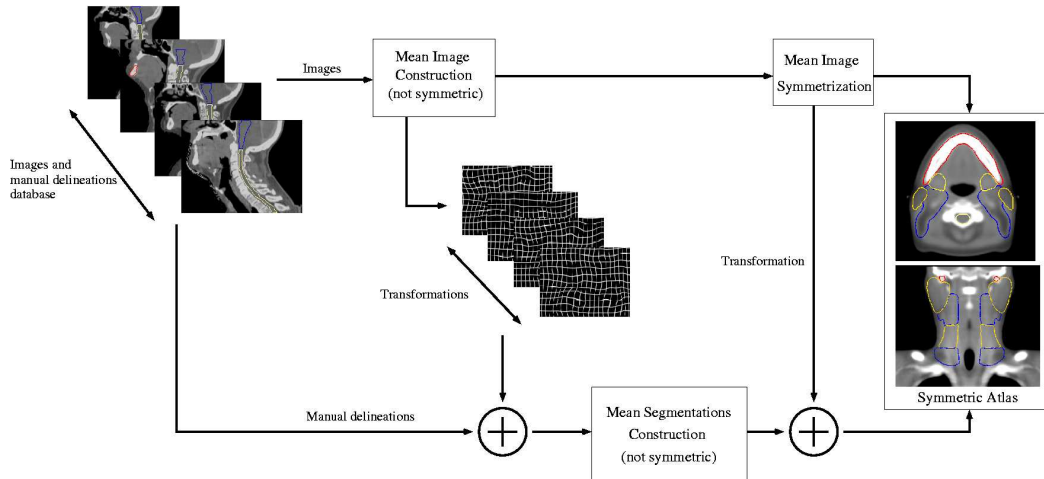


Fig. 2. **Schematic view of the symmetric atlas construction method.** This scheme illustrates the major steps (mean image construction, mean segmentations computation and symmetrization) used to build an atlas from a dataset of images.

### 2.2.3 Mean Image Construction

This first step is performed using the method developed by Guimond *et al.* [19]. It has the advantage of being faster and simpler than the one proposed by Lorenzen *et al.* [21] and is sufficient for our images. This method is based on an iterative scheme to build an unbiased mean image from the image database.

At each iteration  $i$ , all the images  $I_k$  are non linearly registered (details are given in section 2.3.2) on a reference image  $R_i$ , deriving transformations  $T_k$ . Next, a mean image  $M_i$  is built by averaging the intensities of the registered images. At the same time, the non linear transformations  $T_k$  are averaged to produce a transformation  $\bar{T}$ . The reference image for the next iteration is then computed by applying its inverse to  $M_i$ :  $R_{i+1} = M_i \circ \bar{T}^{-1}$ .

Once convergence is reached, a mean image  $\tilde{M}$  is obtained as well as transformations  $\tilde{T}_k$  deforming each image  $I_k$  on  $\tilde{M}$ . At the outset this algorithm requires an initial reference image  $R_0$ . As the built atlas is unbiased, any image of the database can be selected as  $R_0$ . More details can be found in [19].

### 2.2.4 Mean Segmentations Computation

Each image  $I_k$  is now associated to one transformation  $\tilde{T}_k$  bringing it on the mean image  $\tilde{M}$ . By applying these  $\tilde{T}_k$  transformations to the manual segmentations, we can then obtain all the manual segmentations on  $\tilde{M}$ .

The classical approach to obtaining the mean segmentations consists in taking the average of the manual segmentations independently for each structure. However, a high variability exists among the patients in the database, which can result in registration discrepancies. This may have an important impact on the average segmentations when using a simple mean. Moreover, using a simple mean may produce overlapping mean segmentations for structures that are in close proximity. This is not satisfactory as they are assumed to be separated.

To overcome these drawbacks, we have chosen to use STAPLE [26]. This method uses a set of segmentations to produce a robust multi-category “ground truth”. This is done using an Expectation Maximization algorithm iterating the following steps:

- the probability of each voxel to belong to each structure is computed in the Expectation step, knowing the current estimates of the expert parameters,
- quality parameters for each input segmentation are computed in the Maximization step knowing the current estimate of the ground truth.

All the manual segmentations coming from image  $I_k$ , and transformed onto the mean image  $\tilde{M}$ , are used as the input segmentations in STAPLE. Next, the mean segmentations are computed by using a classification of the obtained probabilities (i.e. each voxel is assigned the class that has the highest probability). This therefore ensures separated mean segmentations. Moreover, the EM algorithm ensures a better robustness with respect to variations among the manual segmentations due to misregistrations, intra- or inter-expert variability.

### 2.2.5 Atlas Symmetrization

The preceding steps aimed at building an asymmetric mean image and its associated mean segmentation. As previously indicated, using a symmetric atlas will help avoiding discrepancies when registering it on the patients. We are thus interested in this section in symmetrizing the atlas obtained above.

To this end, we have chosen to use a method which estimates the transformation bringing the image on its symmetry plane. This method is illustrated in the literature on the computation of the mid-sagittal plane of the brain [27]. Briefly, this method looks iteratively for a transformation  $R$  between the

image  $I$  and its symmetric  $I \circ S_K$ , where  $S_K$  is a mirroring transformation. Additional details regarding this algorithm are presented in [27].

The mean symmetric image  $\tilde{M}_S$  is then computed by averaging the mean image centered on its symmetry plane  $\tilde{M} \circ R$  and its symmetric  $\tilde{M} \circ R \circ S_K$ . The binary symmetric segmentations are then obtained in two steps:

- the symmetrization is applied to the image of probabilities from STAPLE,
- then, the symmetric probabilities are classified to get the mean symmetric binary segmentations.

### 2.3 Atlas Adaptation

In the previous sections, we have presented a method for building an anatomical atlas, composed of a mean CT image and of mean segmentations, from a database of images. The next step in the proposed atlas-based segmentation method is to adapt this atlas onto the patient to produce its automatic segmentation.

#### 2.3.1 Adaptation Process

Given the atlas  $\tilde{M}_S$  and a patient  $P$ , atlas-based segmentation relies on a two-step inter-patient registration process:

- a global affine transformation is computed between  $P$  and  $\tilde{M}_S$ , based on a robust Block-Matching registration algorithm [28],
- then, the remaining local deformations due to inter-patient variability are recovered using a non linear registration method.

These transformations are then applied to the atlas structures to produce the automatic delineations. The non linear registration method is crucial to get an accurate segmentation of the patient. There is indeed a tradeoff between its robustness and its ability to recover the deformations due to inter-patient variability.

#### 2.3.2 Non Linear Registration Method

To get the best trade-off between robustness and precision, we have presented in [29] a framework to evaluate both the method used to build the atlas and the one to register it on the patient. This study, performed on three different methods, has shown better results when using a two steps hierarchical approach for both the atlas construction and the atlas registration.

- First, locally affine registration [30] is used to recover the large displacements in a robust manner.
- Then, the remaining local deformations are recovered using a dense transformation (one displacement vector per voxel).

Locally affine registration [30] allows predefined regions to be registered on a reference image by associating to each region a local affine transformation. The global transformation is then interpolated between the regions using weight functions for each region. The transformation is optimized by alternating between the optimization and a visco-elastic regularization of the affine transformations. More details can be found in [30]. In our context, regions were defined on the structures that were available to build the atlas.

The second step is then to optimize a dense transformation to recover the remaining local deformations. To be able to recover large anatomical differences while being robust to registration discrepancies, we have chosen to use a method integrating an *a priori* outlier rejection. Moreover, this method is fast and able to produce smooth deformation fields.

This method, also presented in [29], is an extension to dense transformation of Block-Matching based rigid registration [28]. At each iteration  $i$ , pairings are computed between the images using Block-Matching. A correction displacement field  $\delta T$  is then interpolated from the sparse pairings  $U_i$  using the similarity values of the pairings as confidence parameters. This ensures a smooth transformation close to the pairings associated to a good confidence value, and more interpolated anywhere else.

An outlier rejection is then performed by comparing  $\delta T$  and  $U_i$ . If the norm of their difference is greater than an automatically defined threshold, then the pairing is considered as an outlier and removed. A correction  $\delta \tilde{T}$  is then computed from the remaining pairings and composed with the current estimate of the transformation.

#### 2.4 Atlas Evaluation

We have presented so far a method for constructing an atlas from a database of manually segmented images. We now present a framework to evaluate the quality of the automatic delineation on our database. This process consists of the following steps:

- one of the database images and its segmentation is set aside
- the atlas is built from the  $N - 1$  other images (see section 2.2)
- the atlas is adapted on the left-out patient (see section 2.3.1)
- comparison of the automatic and manual segmentations

Two common overlap-based measures were used to compare the automatic and manual segmentations: sensitivity and specificity. We also compute the error between this couple of measures and the best achievable result (Sensitivity = 1, Specificity = 1), defined as the norm  $\|(1 - Sens., 1 - Spec.)\|$ . This error has no unit and gives a simplified idea of the quality of the result. The overall quality of the automatic segmentation indeed increases as the error decreases.

### 3 Results

In this section, we present the segmentation results produced by the atlas built from our database of images. We will then first present the atlas which is obtained from our construction process. Then, we will present qualitative and quantitative results on the database of images presented in section 2.1.

#### 3.1 Obtained Atlas

We have used our symmetric atlas construction method to build an atlas from the database of 45 CT images described in section 2.1. Fig. 3 illustrates this atlas, showing the mean delineations superimposed on the mean image.

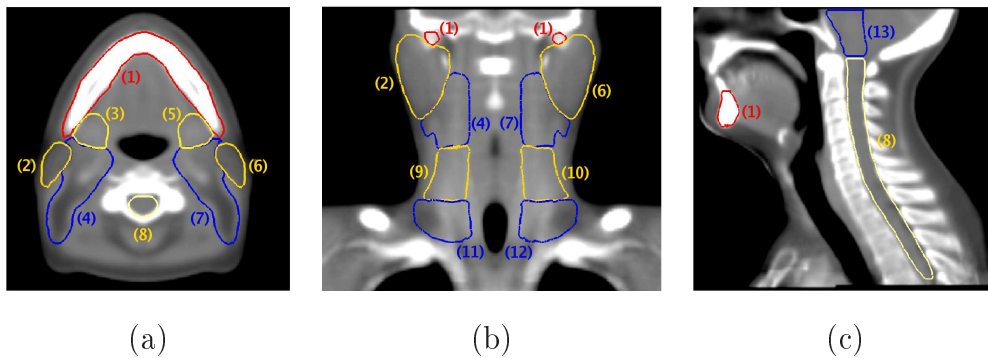


Fig. 3. **Resulting atlas using our symmetric construction method.** Contours of mean structures superimposed on the mean image of the atlas: (a): axial slice, (b): coronal slice, (c): sagittal slice. Structures represented in the atlas: (1) : mandible ; (2) : right parotid ; (3) : right sub-mandibular gland ; (4) : right level II ; (5) : left sub-mandibular gland ; (6) : left parotid ; (7) : left level II ; (8) : spinal cord ; (9) : right level III ; (10) : left level III ; (11) : right level IV ; (12) : left level IV ; (13) : brainstem.

First, this figure shows that the registration method used in the atlas construction process performs well. Indeed, we were able to produce images with sharp vertebral boundaries (image (c)), even though this region was particularly variable among the patients of the database (see Fig. 1). Our technique

of hierarchical non linear registration seems then well adapted for the atlas construction.

Images (a) and (b) also reveal certain structures, such as parotids and lymph node levels II, that are slightly over-segmented, which is primarily due to the variability in the manual segmentations among the various patients in the database. Even after non linear registration on the mean image, when the structures have been visually well deformed to correspond to those of the atlas, these structures are still different. This intra-expert inter-patient variability therefore results in an overestimation when computing the mean segmentations. The structures, however, are still very close qualitatively to the segmentations which we would expect.

### 3.2 Qualitative Evaluation

In Fig. 4, we show the qualitative results obtained on a patient left-out of the database using our Leave-One-Out evaluation method, the results of which were compared to the manual segmentations available for this left-out patient.

First, on structures such as the brainstem, spinal cord or mandible, we see that the delineations are qualitatively good when compared to the manual segmentations. However, we also note a slight over-segmentation of the lymph node levels (particularly level II) and of the parotids. There are indeed some of the surrounding tissues that are included in node level II (see arrows on coronal slices (b) and (e)). These oversegmentations are linked to the ones we have noticed in the atlas. They may also be linked to registration discrepancies that arise when deforming the atlas on the patient. These errors can be due to too large differences in the amount of neck fat as well as position differences between the patient and the atlas.

### 3.3 Quantitative Evaluation

The quantitative evaluation of the atlas-based segmentation was performed using the method proposed in section 2.4 on 12 patients in the database. This subset was chosen so that most of the atlas structures were manually delineated on each patient. The evaluation on this subset will then allow to get a better view of the results obtained by the atlas-based segmentation.

In Table 1, we present the sensitivity and specificity results obtained for these patients. For clarity, we show only the mean results over all structures of each patient. For each couple of sensitivity/specificity results, we also show the error between this pair and the best achievable result (Sensitivity = 1,

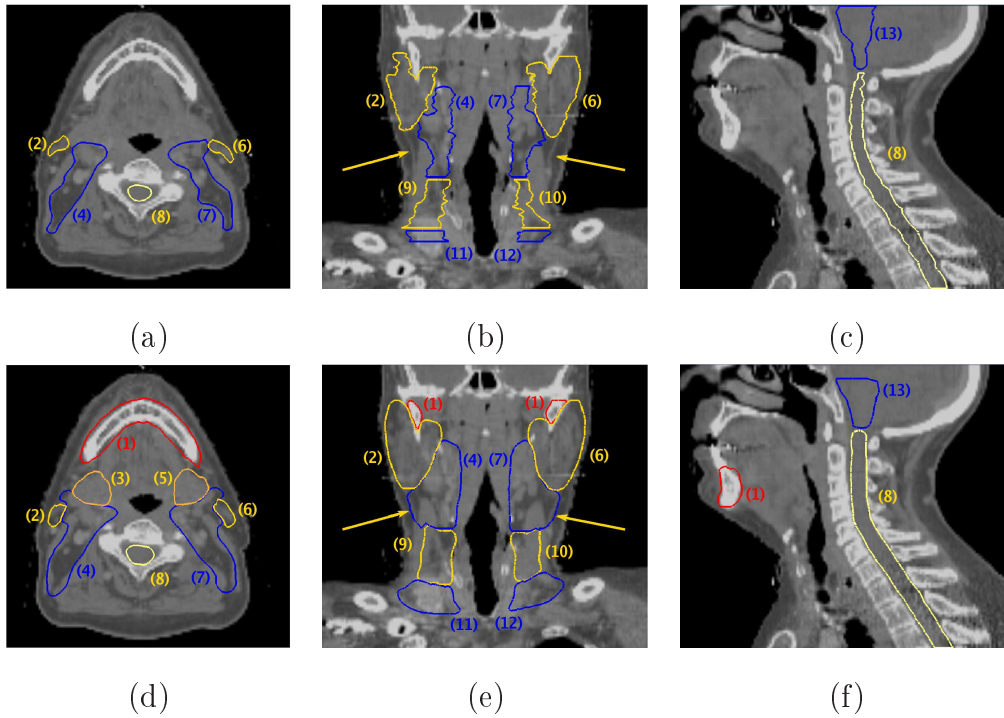


Fig. 4. **Qualitative comparison of the atlas-based and manual segmentations.** Delineations obtained on a patient removed from the atlas construction process using the Leave-One-Out method. (a), (b), (c): manual segmentations ; (d), (e), (f): delineations obtained using the atlas. Structures represented: (1) : mandible ; (2) : right parotid ; (3) : right sub-mandibular gland ; (4) : right level II ; (5) : left sub-mandibular gland ; (6) : left parotid ; (7) : left level II ; (8) : spinal cord ; (9) : right level III ; (10) : left level III ; (11) : right level IV ; (12) : left level IV ; (13) : brainstem.

Specificity = 1), (see section 2.4). Finally, the overall mean of these results over the 12 patients is shown (bold line in the table).

This table indicates that the results are good for almost all patients. We indeed obtain errors ranging from 0.196 to 0.404, and the overall mean error is of 0.253, which suggests our atlas performs well on our database. One patient (patient 9), however, was not as well delineated as the others. This is due to the specific anatomy of this patient, who was particularly large. His anatomy is indeed very different from the one of the atlas as it can be seen in Fig. 5.

This figure is a clear illustration that large differences can exist between some patients and the mean atlas. This, in turn, can lead to registration discrepancies, giving therefore less good quantitative results. This observation suggests the presence of sub-populations within the database. One possible solution to this problem would then be to build several atlases representing these sub-populations from the image database. Then, by selecting the most similar atlas to a given patient, the anatomical differences would be less important and the results closer to the manual segmentations.

	Sens.	Spec.	Error		Sens.	Spec.	Error
<b>Mean</b>	<b>0.820</b>	<b>0.860</b>	<b>0.253</b>	Patient 7	0.872	0.838	0.223
Patient 1	0.852	0.870	0.216	Patient 8	0.888	0.842	0.203
Patient 2	0.853	0.855	0.228	Patient 9	0.636	0.865	<b>0.404</b>
Patient 3	0.793	0.849	0.277	Patient 10	0.738	0.901	0.291
Patient 4	0.911	0.829	0.211	Patient 11	0.892	0.814	0.234
Patient 5	0.740	0.876	0.307	Patient 12	0.776	0.924	0.240
Patient 6	0.890	0.860	<b>0.196</b>				

Table 1. **Quantitative results of atlas-based segmentation.** Mean sensitivity (Sens.), specificity (Spec.) and error with respect to the best result achievable ( $Sens. = 1, Spec. = 1$ ) on twelve patients (between 10 and 13 structures delineated manually for each patient). The mean row corresponds to the average of the results over the twelve patients. Bold figures show the overall average results as well as the lowest and highest errors obtained on the 12 patients.

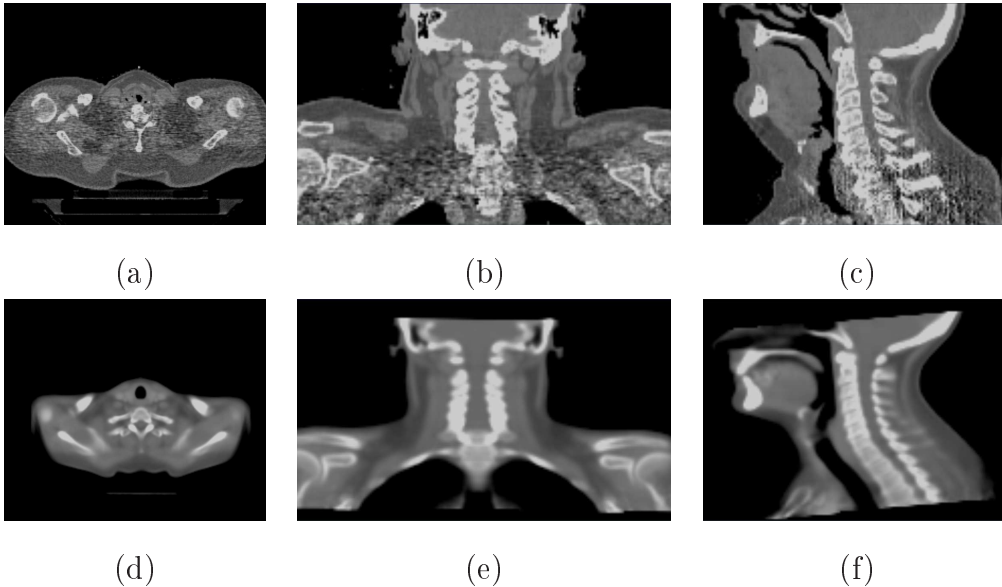


Fig. 5. **Comparison between the atlas and a corpulent patient.** Illustration of the anatomy differences between the atlas (bottom line) and patient 9 (upper line) after a global affine registration.

#### 4 Discussion

In this article, we have presented a method for creating an anatomical atlas of the head and neck region from a database of 45 manually delineated CT images. This method was associated with a Leave-One-Out framework to quantitatively evaluate the results of the atlas-based segmentation. The

evaluation of the built atlas has shown good results both qualitatively and quantitatively. This demonstrates the feasibility of using an anatomical atlas for radiotherapy planning in this region, producing fully automatic and reproducible segmentations of the structures of interest.

The atlas built in this article already includes many useful structures for radiotherapy planning. However, there are still structures that are not present in the database of images. A first additional work to this article will then be to get more structures delineated in the database to get an atlas comprising all the structures needed for radiotherapy, as described in [11].

Then, more validation is also to be added to this work and particularly in clinical conditions. It would indeed be of great interest to compare the results of the atlas on patients from different centers. Moreover, a cross validation from several experts would be very important. Efforts to reach this validation actually have begun within the MAESTRO European project [31], where the automatic segmentations of several patients were compared to several manual segmentations from different experts. This study, that needs to be extended to more patients and more experts, confirmed our results showing an over-segmentation of some structures and quantifying an inter- and intra-expert variability of the manual segmentations. However, the obtained structures are still very well located and could be used in the future as initialization for post-processing algorithms, for example constrained deformable models.

Other issues concern the atlas construction method itself. For example, we have seen in our experiments that the structures were overly-segmented inside the atlas itself. This is likely owing to the intra-expert variability in the manual delineations. Such variability can result in too large average segmentations. Hence, the process chosen for building the mean segmentations from the individual ones may not be optimal. It would therefore be interesting to evaluate quantitatively this intra-expert variability. The evaluation of different methodologies to build the mean delineations, that can take into account probabilistic manual segmentations instead of binary ones, will also be interesting. These could be for example a combination of [32] with the Log-Odd maps [33].

As previously mentioned, an other source of errors explaining the over segmentations are the large differences existing between the patients in the database. Indeed, variable amounts of fat in the neck region as well as the position of the neck relative to the atlas can also result in registration discrepancies. One solution to this problem could be the construction of several atlases tailored to the sub-populations in the image database, as proposed in [34]. A challenging point will then be the selection for a given patient of the most similar atlas to get the best segmentation results.

The built atlas described in this paper has been aimed at patients with tumors staged N0, i.e. tumors that do not deform the anatomy. Consequently, this atlas may fail to segment patients with node-positive tumors, that may induce a large deformation of the nearby structures. The construction of atlases for patients with tumors of higher stages will then be of great importance. This also implies to take into account for the deformations caused by the tumor in the images when building the atlas and when registering it.

## Acknowledgments

This work was partially founded by ECIP project MAESTRO (IP CE503564) and ANRT. The authors are also grateful to Dr. Simon K. Warfield and to Nancy Drinan from Childrens Hospital Boston for their very helpful remarks on this article.

## References

- [1] Gee J.C., Reivich M., Bajcsy R.. Elastically deforming a three-dimensional atlas to match anatomical brain images. *Journal of Computer Assisted Tomography* 17 (2) (1993) 225–236.
- [2] Collins D.L., Holmes C.J., Peters T.M., Evans A.C.. Automatic 3-D model-based neuroanatomical segmentation. *Human Brain Mapping* 3 (3) (1995) 190–208.
- [3] Iosifescu D.V., Shenton M.E., Warfield S.K., Kikinis R., Dengler J., Jolesz F.A., McCarley R.W.. An automated registration algorithm for measuring MRI subcortical brain structures. *NeuroImage* 6 (1) (1997) 13–25.
- [4] Musse O., Heitz F., Armspach J.-P.. Fast deformable matching of 3D images over multiscale nested subspaces. Application to atlas-based MRI segmentation. *Pattern Recognition* 36 (8) (2003) 1881–1899.
- [5] Dawant B. M., Hartmann S. L., Thirion J-P., et al. Automatic 3-D segmentation of internal structures of the head in MR images using a combination of similarity and free-form transformations: Part I, methodology and validation on normal subjects. *IEEE Transactions on Medical Imaging* 18 (10) (1999) 909–916.
- [6] D’Haese P., Niermann K., Cmelak A., Donnelly E., Duay V., Li R., Dawant B.. Neuroanatomical automatic segmentation in brain cancer patients. *International Journal of Radiation Oncology Biology Physics* 57 (2) (2003) S205.
- [7] Bondiau PY, Malandain G, Chanalet S, et al. Atlas-based automatic segmentation of MR images: validation study on the brainstem in radiotherapy context. *Int J Radiat Oncol Biol Phys* 61 (1) (2005) 289–98.

- [8] Dawant B M, Hartmann S L, Pan Shiyang, Gadamsetty S. Brain atlas deformation in the presence of small and large space-occupying tumors. *Computer Aided Surgery* 7 (1) (2002) 1–10.
- [9] Bach Cuadra M, Pollo C, Bardera A, Cuisenaire O, Villemure J, Thiran J. Atlas-based segmentation of pathological MR brain images using a model of lesion growth. *IEEE Transactions on Medical Imaging* 23 (10) (2004) 1301–1314.
- [10] Bach Cuadra M, De Craene M, Duay V, et al. Dense Deformation Field Estimation for Atlas-based Segmentation of Pathological MR Brain Images. *Computer Methods and Programs in Biomedicine* 84 (2-3) (2006) 66–75.
- [11] Grégoire V, Levendag P, Ang K, et al. CT-based delineation of lymph node levels and related CTVs in the node-negative neck: DAHANCA, EORTC, GORTEC, NCIC, RTOG consensus guidelines. *Radiother Oncol* 69 (3) (2003) 227–36.
- [12] Grégoire V, Eisbruch A, Hamoir M, et al. Proposal for the delineation of the nodal CTV in the node-positive and the post-operative neck. *Radiother Oncol* 79 (1) (2006) 15–20.
- [13] Cocosco CA, Kollokian V, Kwan RKS, et al. BrainWeb: Online interface to a 3D MRI simulated brain database. *NeuroImage* 5 (4) (1997) S425.
- [14] Kwan RKS, Evans AC, Pike GB. MRI simulation-based evaluation of image-processing and classification methods. *IEEE Transactions on Medical Imaging* 18 (11) (1999) 1085–97.
- [15] Kwan RKS, Evans AC, Pike GB. An extensible MRI simulator for post-processing evaluation. In: *Visualization in Biomedical Computing (VBC'96)*. Vol. 1131 of LNCS. 1996. pp. 135–140.
- [16] Collins DL, Zijdenbos AP, Kollokian V, et al. Design and construction of a realistic digital brain phantom. *IEEE Transactions on Medical Imaging* 17 (3) (1998) 463–468.
- [17] Marsland S, Twining CJ, Taylor CJ. Groupwise non-rigid registration using polyharmonic clamped-plate splines. In: *Med Image Comput Comput Assist Interv*. Vol. 2879 of LNCS. Springer, 2003. pp. 771–779.
- [18] Park H, Bland PH, Hero AO, et al. Least biased target selection in probabilistic atlas construction. In: *Med Image Comput Comput Assist Interv*. Vol. 3750 of LNCS. Springer, 2005. pp. 419–426.
- [19] Guimond A, Meunier J, Thirion JP. Average brain models: A convergence study. *Computer Vision and Image Understanding* 77 (2) (2000) 192–210.
- [20] Joshi S, Davis B, Jomier M, et al. Unbiased diffeomorphic atlas construction for computational anatomy. *Neuroimage* 23 Suppl 1 (2004) S151–60.
- [21] Lorenzen P, Davis B, Joshi SC. Unbiased atlas formation via large deformations metric mapping. In: *Med Image Comput Comput Assist Interv*. Vol. 3750 of LNCS. Springer, 2005. pp. 411–418.

- [22] Grabner G, Janke AL, Budge MM, et al. Symmetric atlasing and model based segmentation: An application to the hippocampus in older adults. In: *Med Image Comput Comput Assist Interv.* Vol. 4191 of LNCS. Springer, 2006. pp. 58–66.
- [23] Studholme C. Simultaneous population based image alignment for template free spatial normalisation of brain anatomy. In: *Workshop on Biomedical Image Registration.* Vol. 2717 of LNCS. Springer, 2003. pp. 81–90.
- [24] Bhatia KK, Hajnal JV, Puri BK, et al. Consistent groupwise non-rigid registration for atlas construction. In: *International Symposium on Biomedical Imaging.* 2004. pp. 908–911.
- [25] De Craene M, duBois d’Aische A, Macq B, et al. Multi-subject registration for unbiased statistical atlas construction. In: *Med Image Comput Comput Assist Interv.* Vol. 3217 of LNCS. Springer, 2004. pp. 655–662.
- [26] Warfield SK, Zou KH, Wells WM. Simultaneous truth and performance level estimation (STAPLE): an algorithm for the validation of image segmentation. *IEEE Transactions on Medical Imaging* 23 (7) (2004) 903–21.
- [27] Prima S, Ourselin S, Ayache N. Computation of the mid-sagittal plane in 3D brain images. *IEEE Transactions on Medical Imaging* 21 (2) (2002) 122–138.
- [28] Ourselin S, Roche A, Prima S, et al. Block matching: A general framework to improve robustness of rigid registration of medical images. In: *Med Image Comput Comput Assist Interv.* Vol. 1935 of LNCS. Springer, 2000. pp. 557–566.
- [29] Commowick O, Malandain G. Evaluation of atlas construction strategies in the context of radiotherapy planning. In: *Proceedings of the SA2PM Workshop (From Statistical Atlases to Personalized Models).* Copenhagen, 2006. Held in conjunction with MICCAI 2006.
- [30] Commowick O, Arsigny V, Costa J, et al. An efficient locally affine framework for the registration of anatomical structures. In: *International Symposium on Biomedical Imaging.* 2006. pp. 478–481.
- [31] Isambert A., Grégoire V., Bidault F., Calais G., Commowick O., Malandain G., Ruaud J.B., Tomsej M., Bramouille C., Bourhis J., Lefkopoulos D.. Atlas-based automatic segmentation (ABAS) of head and neck (H&N) structures in conformal radiotherapy (CRT): atlas development and preliminary results in clinical context. In: *Acts of the 26th European Society for Therapeutic Radiology and Oncology (ESTRO 2007).* 2007.
- [32] Warfield SK, Zou KH, Wells WW. Validation of image segmentation by estimating rater bias and variance. In: *Med Image Comput Comput Assist Interv.* Vol. 4191 of LNCS. Springer, 2006. pp. 839–847.
- [33] Pohl KM, Fisher J, Shenton M, et al. Logarithm odds maps for shape representation. In: *Med Image Comput Comput Assist Interv.* Vol. 4191 of LNCS. Springer, 2006. pp. 955–963.

- [34] Blezek DJ, Miller JV. Atlas stratification. In: Proc. of the 9th International Conference on Medical Image Computing and Computer Assisted Intervention (MICCAI'06), Part I. Vol. 4190 of LNCS. Springer, 2006. pp. 712–719.